PROCEEDINGS OF SPIE

SPIEDigitalLibrary.org/conference-proceedings-of-spie

Improved electromagnetic induction processing with novel adaptive matched filter and matched subspace detection

Charles Ethan Hayes
James H. McClellan
Waymond R. Scott
Andrew J. Kerr

SPIE.

Improved electromagnetic induction processing with novel adaptive matched filter and matched subspace detection

Charles Ethan Hayes, James H. McClellan, Waymond R. Scott, Jr., and Andrew J. Kerr

School of Electrical and Computer Engineering, Georgia Institute of Technology,
Atlanta, GA, USA 30332-0250

ABSTRACT

This work introduces two advances in wide-band electromagnetic induction (EMI) processing: a novel adaptive matched filter (AMF) and matched subspace detection methods. Both advances make use of recent work with a subspace SVD approach to separating the signal, soil, and noise subspaces of the frequency measurements.[1] The proposed AMF provides a direct approach to removing the EMI self-response while improving the signal to noise ratio of the data. Unlike previous EMI adaptive downtrack filters, this new filter will not erroneously optimize the EMI soil response instead of the EMI target response because these two responses are projected into separate frequency subspaces. The EMI detection methods in this work elaborate on how the signal and noise subspaces in the frequency measurements are ideal for creating the matched subspace detection (MSD) and constant false alarm rate matched subspace detection (CFAR) metrics developed by Scharf.[2] The CFAR detection metric has been shown to be the uniformly most powerful invariant detector.

Keywords: Electromagnetic induction, adaptive matched filter, matched subspace detection, constant false alarm rate, magnetic soil, subspace interference seperation

1. INTRODUCTION

This work introduces two advances in wide-band electromagnetic induction (EMI) processing: a novel adaptive matched filter (AMF) and a constant false alarm rate matched subspace detector. Both advances make use of recent work with a subspace SVD approach to separating the signal, soil, and noise subspaces of the frequency measurements.[1] The AMF removes the EMI sensor self-response while improving the signal to noise ratio (SNR) of the EMI data. The AMF builds a downtrack filter by maximizing the strength of the signal space while constraining the spatial wavelength response of the downtrack filter. The sensor self-response is removed by forcing the constant spatial component to be zero, and noise/interference is reduced by nulling short spatial wavelength components that are not from EMI targets. Unlike previous EMI adaptive downtrack filters, this new filter will not erroneously optimize the EMI soil response instead of the EMI target response because these two responses are projected into separate frequency subspaces.

This work shows how the signal, soil, and noise frequency subspaces are ideal for defining a matched subspace detection (MSD) and constant false alarm rate match subspace detection (CFAR) metrics defined in Ref. 2. The CFAR metric was proven to have a generalized likelihood ratio test that is the uniformly most powerful invariant detector.[2] This new EMI detection method will be tested with the proposed AMF, as well as other downtrack filters, on field data to compare their effectiveness.

This paper will be organized as follows. The first section will describe the model for a wide-band EMI sensor. The following section will discuss the downtrack filtering stage in EMI processing and will focus on three topics: discuss the purpose of EMI downtrack filters, review some of the current filter options, and finally introduce the proposed AMF and provide results. The third section will focus on the EMI detection problem. This section reveals the direct application of the MSD and CFAR detector followed by a comparison of results between detection methods and downtrack filter pairings. A fourth section provides a glimpse into the future work on this field and is accompanied by initial results for detection.

Further author information: (Send correspondence to Charles Ethan Hayes)
E-mail: chayes30@gatech.edu, jim.mcclellan@ece.gatech.edu, waymond.scott@ece.gatech.edu, and dkerr3@gatech.edu

Detection and Sensing of Mines, Explosive Objects, and Obscured Targets XXI,
edited by Steven S. Bishop, Jason C. Isaacs, Proc. of SPIE Vol. 9823, 98230E
 · doi: 10.1117/12.2224681

2. GENERAL MODEL

2.1 Creating the Measurement Matrix

This work focuses on improving processing methods for a wide-band frequency-domain EMI sensor designed to find targets buried below the ground. The EMI sensor operates by moving over a region of interest and taking measurements at discrete positions along its path. Each EMI measurement consists of a small set of frequency-domain samples. For the Georgia Tech EMI platform that is used as the base platform in this work, there are 21 frequencies resulting in 21 complex measurements for each position. This acquisition process can be described as a function of two parameters, position and frequency, and the EMI sensor data can be written as

$$M(\omega, p) \tag{1}$$

where p denotes the location of the EMI sensor at the time of the measurement and ω is the frequency at which a measurement sample was taken.

By combining a series of frequency samples through position, a measurement matrix can be created such that

$$\hat{\mathbf{M}} = [M(\omega_i, p_j)]_{i,j} \tag{2}$$

where ω_i is the i^{th} frequency and p_j is the j^{th} position. This produces a measurement matrix $\hat{\mathbf{M}} \in \mathfrak{C}^{n \times l}$ where n frequencies were sampled at l positions. In order to account for a continuously moving EMI sensor, the p would be continually shifted through space to contain the latest l positions. In other words, any processing that is applied to what will be denoted as the downtrack dimension can be interpreted as an l-tap filter.

Because the proposed EMI processing does not alter phase information between measurements and aims to combine the data in a coherent way, the real and imaginary parts of the measurements will be separated in order to create a real matrix. This operation is performed by concatenating the real and imaginary parts of each complex frequency measurement into a column vector of twice the length, as shown in

$$\mathbf{M} = \begin{bmatrix} \Re(\hat{\mathbf{M}}) \\ \Im(\hat{\mathbf{M}}) \end{bmatrix} \tag{3}$$

where $\mathbf{M} \in \Re^{2n \times l}$ becomes the final data matrix that will be used in this work.

2.2 Model Sources

Now that the measurement matrix is defined, the next step will be to investigate the model that describes the data. The measurements $\mathbf{M}$ have four major components and can be modeled as

$$\mathbf{M} = \mathbf{S} + \mathbf{G} + \mathbf{R} + \mathcal{E} \tag{4}$$

where $\mathbf{S}$ is the desired signal response from a target, $\mathbf{G}$ is an interference signal from the soil response, $\mathbf{R}$ is the self-response of the EMI sensor, and $\mathcal{E}$ is additive random noise with each element being an i.i.d. $N(0, \sigma^2)$ random normal variable.

The soil response originates from the fact that most soils contain some degree of ferrous particles that can be detected by the EMI sensor. This soil response varies based on ω, and empirical studies[3] have shown that it can be estimated in a 2-dimensional vector space

$$G(\omega) = \begin{bmatrix} 1 & \log(\frac{\omega}{\omega_c}) + \frac{j\pi}{2} \end{bmatrix} \tag{5}$$

where ω_c is a model frequency parameter and $G \in \mathfrak{C}^{n \times 2}$ when n frequency samples are taken. The columns of G when stacked into a real matrix, as in (3), can be made orthogonal by choosing the frequency parameter ω_c to be the geometric mean $\omega_c = \Pi_{i=1}^{n} \sqrt[n]{\omega_i}$.

The self-response is an artifact of the coupling between the transmitter and receiver coils on the EMI platform. Even after hardware methods are used to reduce this coupling, the self-response is often around 60 dB stronger

than the weakest detectable target. The coupling is a strong function of frequency ω, but it is essentially constant with respect to position p. This fact allows the self-response to be viewed as a DC component in the downtrack dimension of the data. There does exist a slight amount of variation the downtrack dimension from the coupling due to drift in the system, but this drift is insignificant over the position measurement window that is being used for the downtrack filter.

2.3 Prior Work

This work draws heavily from the authors' previous work[1] which focused on solving the inversion problem of finding the discrete spectrum of relaxation frequencies (DSRF) for a physical target from wide-band EMI frequency samples. In order to more effectively solve this inversion, a system was introduced that used projections to create three subspaces that partition the frequency dimension into a signal, noise, and soil subspace. This system was derived by combining the knowledge of the soil response vector space G in (5) with the eddy current model of a target given by

$$A(\omega, \zeta) = \frac{j\omega/\zeta}{1 + j\omega/\zeta} \tag{6}$$

where ζ is the relaxation frequency of the target. The dictionary of relaxation frequency responses is formed by sampling ζ k times over the measurable relaxation frequency space, using the n measured frequency values ω_i for each ζ_k, and finally separating the real and imaginary parts as was done in (3) to create the dictionary matrix $\mathbf{A} \in \Re^{n \times k}$. After isolating the soil response from the relaxation frequency response dictionary with a projection operator and then applying a singular value decomposition (SVD) on the remaining dictionary, it is possible to rewrite the dictionary as

$$\mathbf{A} = \begin{bmatrix} \mathrm{U}_{\bar{\mathrm{G}}\mathrm{S}} & \mathrm{U}_{\bar{\mathrm{G}}\mathrm{N}} & \mathrm{U}_{\mathrm{G}} \end{bmatrix} \begin{bmatrix} \Sigma_{\bar{\mathrm{G}}\mathrm{S}} & 0 & 0 \\ 0 & \Sigma_{\bar{\mathrm{G}}\mathrm{N}} & 0 \\ 0 & 0 & \Sigma_{\mathrm{G}} \end{bmatrix} \begin{bmatrix} \mathrm{V}_{\bar{\mathrm{G}}\mathrm{S}}{}^{H} \\ \mathrm{V}_{\bar{\mathrm{G}}\mathrm{N}}{}^{H} \\ \mathrm{V}_{\mathrm{G}}{}^{H} \end{bmatrix}. \tag{7}$$

This reformulation resembles a SVD on the original $\mathbf{A}$, but it has no guarantees of V_{G} being orthogonal to the rest of the V terms. The purpose of this reworking is to create three useful projection operators for the frequency dimension of the EMI data. The $\mathrm{U}_{\bar{\mathrm{G}}\mathrm{S}}$ term can be used to project the frequency measurements into a high SNR region that is isolated from soil interference. The $\mathrm{U}_{\bar{\mathrm{G}}\mathrm{N}}$ matrix spans the noise-dominated subspace that is isolated from the soil interference, but there is some level of signal below the noise floor. Finally, the U_{G} term can project the measurements into a subspace that contains the soil as well as some signal and noise. This work will utilize the derived $\mathrm{U}_{\bar{\mathrm{G}}\mathrm{S}}$ and $\mathrm{U}_{\bar{\mathrm{G}}\mathrm{N}}$ terms, while taking advantage of the knowledge that these two spaces are isolated from the soil interference.

3. DOWN-TRACK FILTER

3.1 Purpose

As discussed previously, EMI sensors have a major interference signal created by the self-response of the coils. In order to produce usable measurements from the EMI data, a preprocessing step must be applied to $\mathbf{M}$ in order to remove the self-response $\mathbf{R}$. Because $\mathbf{R}$ is known to resemble a DC component in the downtrack dimension, most processing applications implement a two-stage system that contains an initial downtrack filter followed by any processing desired on the wide-band frequency information. This first stage can be denoted as

$$m = \mathbf{M}\, w \tag{8}$$

where $w \in \Re^{l \times 1}$ is a column vector that contains the downtrack filter coefficients and $m \in \Re^{2n \times 1}$ is a resulting column vector that holds the frequency content over the positions contained in $\mathbf{M}$. The primary goal for creating the coefficients of w is to create a DC rejecting filter that removes the self-response. The filter also serves a second purpose of coherently integrating over multiple samples in order to improve the SNR of the frequency measurements.

3.2 Previous Methods

The standard approach for EMI preprocessing is to create a high-pass downtrack filter that rejects the DC component.[4] This approach can be implemented in either the analog or digital domain. Bruschini investigated multiple variations of high-pass filters, including infinite impulse response (IIR) filters, first and second order derivatives, mean estimation and subtraction, and linear trend removal.[5] Other potential filters listed in Ref. 5 include an adaptive filter that uses the real portion of $\mathbf{M}$ to improve the imaginary portion which is then followed by a Weiner filter, as well as a wavelet transform approach to filtering.

An alternative approach is to use a matched filter for preprocessing in order to improve the SNR of the frequency data as opposed to simply rejecting the interference. A simple approximate matched filter is the sine filter that exploits a property of many modern EMI sensors, such as the Georgia Tech EMI platform, which are equipped with a positive and negative polarized section in the receive coil. As these sensors traverse a target, the response is maximized when it is in the center of the positive section of the receive coil and then decreases to its minimum as it moves to the center of the negative section of the receive coil. An illustration of this effect is shown in Figure 1 in the solid line. Because of this knowledge, it is intuitive to choose a single cycle of a sine wave placed in the middle of the filter with its wavelength equal to double the distance from the center of the two receive coils, as is seen in the dotted red plot. This sine filter also inherently rejects the DC component, as it is zero mean, so it serves well as a downtrack EMI filter. Unfortunately the sine filter does not serve as an exact matched filter because the distance from the coils to the target can alter this basic shape and cause distortions and wavelength changes. Also, if the polarization of the target is not directly up and down, then the response shape can be altered and resemble downtrack response shapes such as the magenta dashed line.

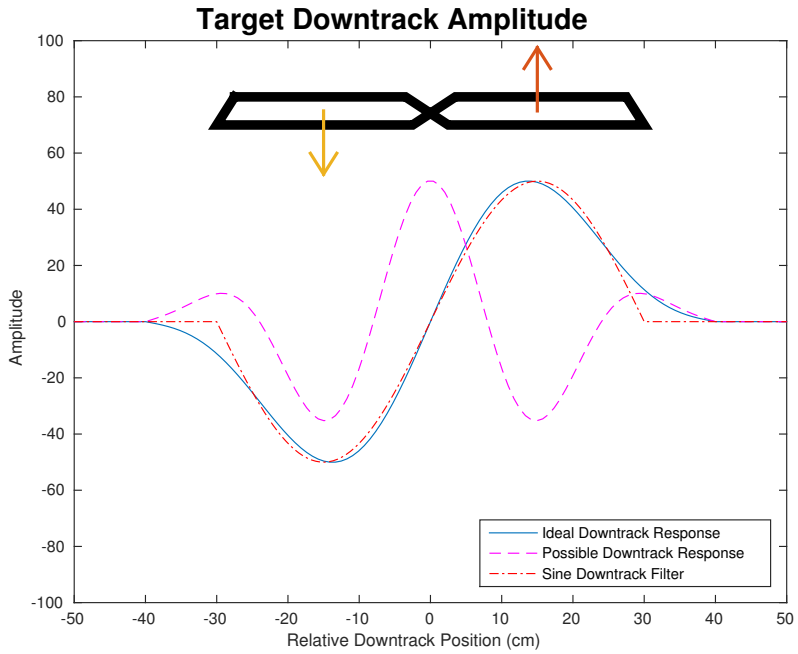

Figure 1. An illustration of the downtrack response as the positive and negative sections of a receive coil pass over a target. The solid blue line represents an ideal downtrack response from a target. The magenta dashed line shows one possible downtrack response when the polarization of the target as well as other environmental variables change. The red dotted plot illustrates the approximation made by the sine filter for approximating a downtrack matched filter.

A recent option is the non-negative adaptive filter (NNAF) proposed by Wei,[6] where an optimization problem is designed to create an optimal filter at each position. This optimization uses knowledge of the eddy currents of a target to encourage that m has a non-negative Discrete Spectrum of Relaxation Frequencies (DSRF)[6] and also enforces a zero mean condition to reject the self-response. The NNAF has been shown to work well for moderately magnetic soils and will serve as the baseline for downtrack filter performance. Although NNAF has been shown to perform well for moderately magnetic soils, it is directly applied to $\mathbf{M}$ that contains the soil

interference and nothing prevents it from optimizing the soil response instead of the target response when the soil overpowers the target. In addition, NNAF was designed to manipulate m for easier DSRF recovery,[7] and the added complexity causes speed deficiencies and provides a challenge for applying the method in real time.

3.3 Adaptive Matched Filter

The objective of the adaptive matched filter (AMF) design is to obtain a coefficient vector $w \in \Re^l$ that is then used as a downtrack filter on the EMI measurements $\mathbf{M}$ as

$$m = \mathbf{M}\, w \tag{9}$$

to produce an output signal m that has maximal signal content as defined in (4) while simultaneously removing the possibility of enhancing the noise or interference terms. By creating a subspace within the measurements that contains the signal with minimal noise and interference, a filter can be produced by maximizing the energy in this subspace. Using the $\mathrm{U}_{\bar{\mathrm{G}}\mathrm{S}}$ defined from previous work,[1] a method for projecting the row space of $\mathbf{M}$ is already defined as $\mathrm{U}_{\bar{\mathrm{G}}\mathrm{S}}{}^H\,\mathbf{M}$. To create the desired signal subspace, it is of interest to find a projector P for the column space such that

$$\mathbf{M}_S = \mathrm{U}_{\bar{\mathrm{G}}\mathrm{S}}{}^H\,\mathbf{M}\,P \tag{10}$$

contains the signal content of $\mathbf{M}$ with minimal noise and interference. Once this subspace is created, the AMF can be adaptively solved by choosing a w that maximizes the amount of energy from $\mathbf{M}_s$ that is contained in the column vector m. For this discussion, it is useful to think of the matrix

$$\mathbf{M}_{Sp} = \mathrm{U}_{\bar{\mathrm{G}}\mathrm{S}}{}^T\,\mathbf{M}\,P(P^TP)^{-1}P^T \tag{11}$$

which is the $\mathbf{M}_S$ matrix that has been projected back into the same downtrack column space as the original $\mathbf{M}$. This allows for w to be created in the p dimension, but it should be noted that for actual processing it will be faster and mathematically equivalent to solve for $\hat{w}$ in the column space of P when possible.

To solve for the AMF, we maximize $\|\,\mathbf{M}_{Sp}\,w\|_2$. This can be done by setting up the optimization problem

$$\begin{aligned} \max_{w} \;& \|\,\mathbf{M}_{Sp}\,w\|_2 \\ \text{s.t. }& \|w\|_2 = 1 \\ \text{s.t. }& \text{constrain sign}(w) \end{aligned} \tag{12}$$

where the constraints guarantee a nonzero unique solution for w. This optimization problem can be solved with the Rayleigh quotient

$$\max_{w} \; \frac{w^T\,\mathbf{M}_{Sp}^T\,\mathbf{M}_{Sp}\,w}{w^Tw} \tag{13}$$

and then declaring a rule for choosing between w or $-w$. The solution of the classic Rayleigh quotient optimization is known to be the eigenvector associated with the largest eigenvalue of $\mathbf{M}_{Sp}^T\,\mathbf{M}_{Sp}$. The sign rule chosen for this work will be

$$w = \text{sign}(e_1^T\,\mathbf{M}_{Sp}\,w_r)w_r \tag{14}$$

where w_r is the solution to the Rayleigh quotient and e_1 is a vector that selects the first element.

This completes the derivation of the AMF, but the problem still remains for selecting a P that is suitable for the EMI downtrack filter. In order for P to be effective, it must be able to isolate the signal from the self response of the sensor. As mentioned before, the self response remains mostly constant throughout the downtrack dimension. This means that as long as P removes the constant component in the column space, then it should be effective. In the following discussion, we will investigate two possible methods for determining P, and then present results from real data where the AMF filter was compared to the optimized filter.

3.3.1 Discrete Fourier Transform Approach

The first method of developing the downtrack projector P is based on the sine filter. In order to create the Discrete Fourier Transform (DFT) approach, define $\mathcal{F}$ as the orthonormal DFT basis matrix. This allows the DFT of the row space of a matrix B to be defined as $\mathcal{F}^T B$ and the DFT of the column space of B would be $B\,\mathcal{F}$. After taking the DFT of the downtrack data, $M\,\mathcal{F}$, the self response is contained in the DC component of the downtrack dimension. Then a matrix $I_S \in \Re^{l\times d}$ can be created that only keeps the d desired wavelengths of the downtrack data.

By using these matrices, it is simple to define

$$P = \mathcal{F}\, I_S \tag{15}$$

which completes (10) as

$$\mathbf{M}_S = {\mathrm{U}_{\bar{\mathrm{GS}}}}^T\, \mathbf{M}\, \mathcal{F}\, I_S \tag{16}$$

where $\mathbf{M}_S \in \mathfrak{C}^{k\times d}$ contains most of the signal energy in $\mathbf{M}$. Note that because the DFT projection $\mathcal{F}$ is complex, this causes the signal subspace matrix $\mathbf{M}_S$ to also be complex. If $\mathbf{M}_S$ is projected back into the downtrack dimension as is done in (11), then it will once again become real. This point is trivial for the discussion here, but should be noted for implementation as it would cause the AMF to perform an eigenvalue decomposition on a complex matrix instead of a real matrix.

In order to complete the DFT AMF, it is necessary to choose which wavelengths to select with I_S. To choose the wavelengths, a Short-Time Fourier Transform (STFT) was applied to EMI data obtained during a test of the Georgia Tech EMI platform. Figure 2 shows the positive frequencies from the STFT of the downtrack dimension, where the frequencies on the vertical axis have been replaced with their corresponding spatial wavelength. For this specific lane of data, there was a metallic object located at markers A, C, D, E, F, H, K, M, and N.

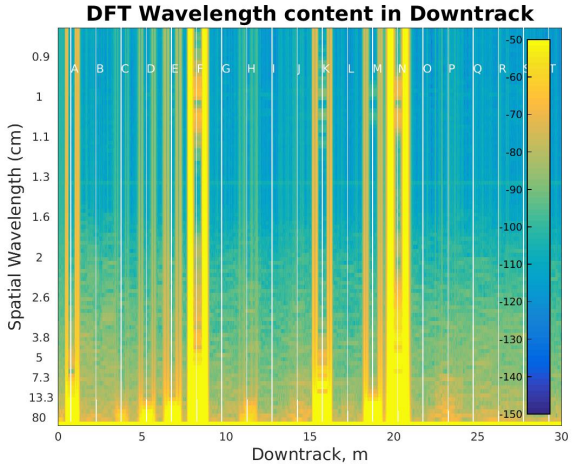

Figure 2. Short Time Fourier Transform of downtrack data for choosing the wavelengths for the DFT AMF. Targets are located at markers A, C, D, E, F, H, K, M, and N.

It can be seen in Figure 2 that most of the signal for each target is contained in wavelengths of 5 cm or larger, except at the edges of the targets when the sharp edge effects can be seen in the DFT across all wavelengths. For this reason, I_S was selected to choose all wavelengths between 5 cm and the length of the filter.

Another point that can be made from Figure 2 is the fact that the self response is shown to nearly completely reside in the DC component of p. This fact was given as foreknowledge about the model, but is confirmed by the STFT of the downtrack data. Any drift that occurs over time is below the target responses and shown to be insignificant.

3.3.2 Discrete Cosine Transform Approach

The filter results in Figure 4 reveal one major flaw in the DFT AMF approach. By observing the downtrack filter created by the DFT AMF, it is easy to notice that the edges of the DFT AMF filter are forced to have the same value. This is an undesirable effect originating from the fact that the DFT is theoretically observing a single period of a periodic signal. Because of this property, the DFT design creates a signal that can be replicated next to itself on either end, which causes the edges of the filter to have equal values. To avoid this edge artifact created by the DFT, a different set of basis functions should be chosen. Other applications that are concerned with these edge effects, such as image processing, have investigated using the Discrete Cosine Transform (DCT). The DCT works on real cosines, and extends the signal with a mirror image before enforcing periodicity. Thus, the DCT does not suffer from the edges of the signal having the same value. The DCT still benefits from having an intrinsic wavelength and sinusoidal shape associated with each basis, which is ideal for the downtrack filter. In addition, the DCT produces real coefficients which allows for further processing on the downtrack dimension to be performed easier. This provides another benefit for the DCT approach over the DFT approach for the downtrack projection operator of the AMF since an eigenvalue decomposition of a real matrix is numerically faster.

The process for developing a P from the DCT basis functions is similar to the DFT method. First, $\mathcal{D}$ is defined as the orthonormal DCT basis matrix with the same definition as $\mathcal{F}$ earlier. A selection matrix $I_S \in \Re^{l \times \hat{d}}$ is defined again to keep the $\hat{d}$ desired cosine frequencies. This allows P to be defined for the DCT AMF approach as

$$P = \mathcal{D}\, I_S \tag{17}$$

and create the measurement signal space as

$$\mathbf{M}_S = \mathrm{U}_{\bar{\mathrm{G}}\mathrm{S}}{}^T\, \mathbf{M}\, \mathcal{D}\, I_S \tag{18}$$

Once again, the selector matrix I_S is chosen by looking at the downtrack DCT obtained from data. Figure 3 shows the DCT of the downtrack dimension performed on the same data set that was used in Figure 2. The DCT, just like the DFT, appears to concentrate the signal information at wavelengths of 5 cm or more. As would be expected, the same wavelength region can be chosen for the DCT selection matrix as was found for the DFT selection matrix. It can also be seen in Figure 3 that the DCT also spreads the signal information across all wavelengths at the edges due to the discontinuous nature of the signal there.

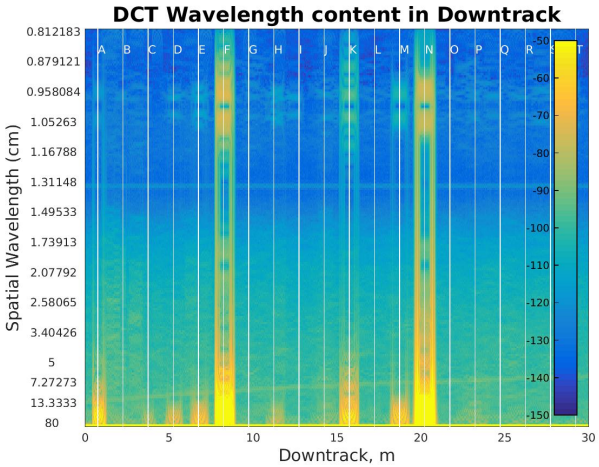

Figure 3. Short Time Discrete Cosine Transform of downtrack data for choosing the wavelengths of the DCT AMF. Targets are located at markers A, C, D, E, F, H, K, M, and N.

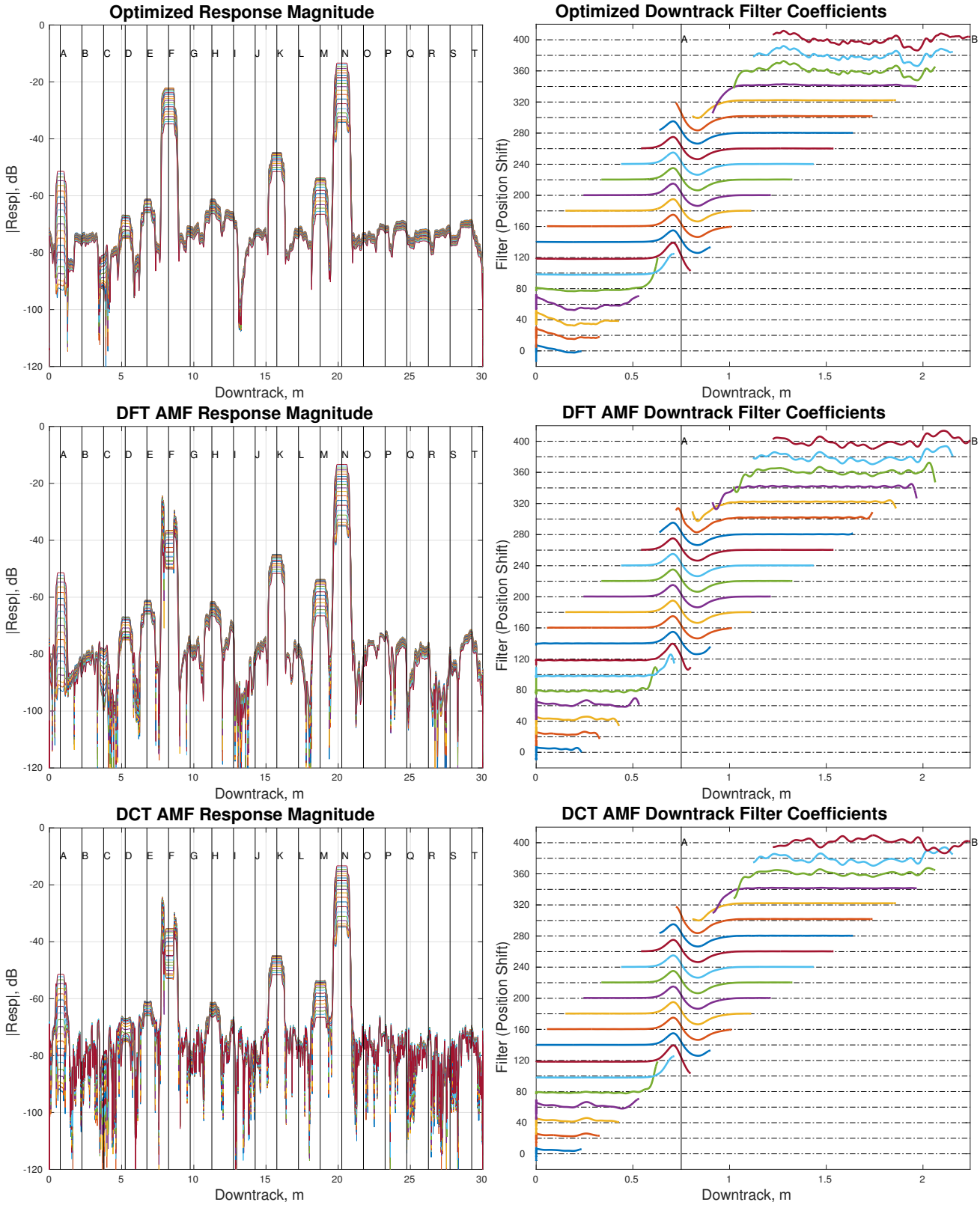

Figure 4. EMI Downtrack filter comparison. The left graphs contain the magnitude of each measurement frequency after the filter has been applied. The right graphs contain a small excerpt where the filter coefficients are displayed as the filter moves over a target. Targets are located at markers A, C, D, E, F, H, K, M, and N.

3.4 Results

In order to determine the effectiveness of the proposed AMF, the downtrack filter is compared directly with the NNAF. The comparison is shown in Figure 4, where the different filters have been used on data obtained by the Georgia Tech Wideband EMI platform. This is the same lane data that was used for the frequency analysis in Figures 2 and 3. The left plots show the magnitude of each of the 21 measured frequencies after the downtrack filter runs on the data. The right plots focus on the beginning of the lane to show how well each filter works with noise and then transitions to fitting a target. All three filters used a window length of roughly 80 cm in order to allow a "flatter" peak on the magnitude graphs as the filters consistently pick the target location as it passes.

It is important to note that both the DFT AMF and DCT AMF are able to improve the target locations to the same degree as the NNAF. Likewise, both AMF filters are able to drive the noise level down to the same level as the NNAF. This shows that the AMF filters can be as effective as the NNAF in distinguishing the targets from the noise. As mentioned previously, the right plots in Figure 4 reveal that the DFT AMF has the undesirable edge effect of causing the ends of the filter to have the same value. This effect can be most clearly seen when the target (A) at 1 m is at the edge of the filter and the other edge is forced to match the ending value. For the DCT AMF filter this edge effect is no longer seen thanks to the DCT basis approach.

All of these adaptive filters are developed around an optimization problem, but when there is no signal present they are forced to optimize the noise to some degree. This leads to a semi-flat look across the downtrack dimension of the magnitudes in the NNAF, including when there is no target. Because the AMF only optimizes over a portion of the noise and P was chosen such that quickly oscillating downtrack filters could not be created, it is more robust to this issue. This is illustrated best at the end of the lane data in the DCT AMF magnitudes. Because the DCT AMF does not always optimize the noise, it oscillates in magnitude when there is no signal. This allows for a clear distinction visually between when there is a target or not.

This comparison between the AMF and NNAF is useful to show that the AMF can work as well as the NNAF. The test data used is fairly ideal in the fact that there is very little soil response contained in it. The NNAF has no way of isolating the soil response, and if the soil response becomes too strong then it has no constraints preventing it from optimizing the soil. The AMF on the other hand isolates the signal from the soil, noise, and self response before performing the optimization. This design would be preferred for scenarios where the soil response is stronger.

4. DETECTION

4.1 Theory

Another important task for EMI processing is to detect when a target is present. The recent work in Ref. 1 provides a clear connection to well developed detection algorithms. This work will focus on developing the connection between the recent SVD separation work in the frequency domain and the established theory of matched subspace detection (MSD) and constant false alarm rate matched subspace detection (CFAR) that was developed in Ref. 2. In Ref. 2, Scharf provides theoretical proofs that state how to make the uniformly most powerful invariant (UMPI) detection system for detecting a signal with multivariate Gaussian distributed noise with a covariance structure that is known but contains an unknown scaling factor, which can be written as $N(0, \sigma^2 R)$ where R is the known covariance structure and σ^2 is an unknown scaling constant. For ease of explanation, this work borrows the notation from Ref. 8 to describe the MSD and CFAR detection methods. The fundamental approach of these works state that if the measurements, m, can be projected in such a way to create

$$z = \begin{bmatrix} z_1 \\ z_2 \end{bmatrix} = \begin{bmatrix} \nu \\ 0 \end{bmatrix} + \epsilon \tag{19}$$

where z_1 contains all of the signal content, denoted as ν, plus a random Gaussian noise term , denoted as ϵ, and z_2 contains only the Gaussian noise term. This is done by pre-whitening the noise of the measurements through the operation $R^{-\frac{1}{2}} m$, where R is the covariance structure of the noise term. After the noise whitening is performed, a subspace projection must be found to create $z = U^T m$.

Once z has been formulated, the values for the associated detection methods can be described as

$$\text{MSD)}\ \gamma = \|z_1\|_2^2 \tag{20a}$$

$$\text{CFAR)}\ \gamma = \frac{\|z_1\|_2^2}{\|z\|_2^2} \tag{20b}$$

where γ is then compared against a trained threshold value in order to determine if a target is present. If these values are greater than the threshold, then it corresponds to a detection. The MSD is the best detection metric when the noise covariance structure and scaling value are known and the CFAR metric is the optimal discriminator for when the covariance structure is known but the scaling can change.

4.2 Application

In order to take advantage of the detection theory provided above, it is necessary to formulate the EMI problem into a similar structure. EMI detection is normally applied on the frequency data after the downtrack filter has been applied. The model for these measurements can be provided by

$$m = \mathbf{M}\, w = \mathbf{S}\, w + \mathbf{G}\, w + \mathcal{E}\, w \tag{21}$$

since the downtrack filter w is responsible for having removed the self response component $\mathbf{R}$. It is easy to see that the additive noise term has now become a multivariate Gaussian distribution that can be defined as $\mathcal{E}\, w \sim N(0, \hat{\sigma}^2 I)$. By then defining $U = [\mathrm{U}_{\bar{\mathrm{G}}\mathrm{S}}, \mathrm{U}_{\bar{\mathrm{G}}\mathrm{N}}]$ as the frequency subspace spanned by the signal and noise spaces orthogonal to the soil response, it allows for an estimate of z to be defined as

$$\hat{z} = U^T\, \mathbf{M}\, w = \begin{bmatrix} \mathrm{U}_{\bar{\mathrm{G}}\mathrm{S}}{}^T\, \mathbf{S}\, w \\ \mathrm{U}_{\bar{\mathrm{G}}\mathrm{N}}{}^T\, \mathbf{S}\, w \end{bmatrix} + \mathcal{E}\, w \approx \begin{bmatrix} \nu \\ 0 \end{bmatrix} + \epsilon\,. \tag{22}$$

The reason $\hat{z}$ only approximates the desired z is because the $\mathrm{U}_{\bar{\mathrm{G}}\mathrm{N}}$ term does not completely remove the signal, but only reduces it below the noise floor. By examining the singular values in Figure 5 that created the projection operator, it can be seen how quickly the signal will drop off in the noise subspace. The results presented in this paper found that stopping the signal dimension at five and nine singular values worked well, which corresponds to the the noise floor being on the order of two and three orders of magnitude smaller than the largest signal component respectively.

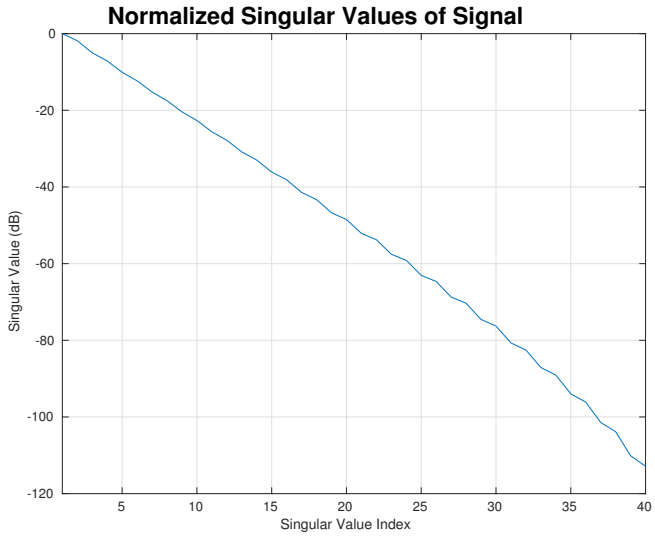

Figure 5. The normalized singular values of the projection matrices that separate the signal from the noise. The signal will be on the order of the singular values compared with the strongest signal term after projected into the space orthogonal to the soil response.

4.3 Results

In order to test the effectiveness of the proposed detection method, an entire data set obtained by the Georgia Tech EMI platform that is described in Ref. 3 was used to analyze the detection capabilities. The Georgia Tech EMI platform obtains 21 complex frequency measurements, which corresponds to $m \in \Re^{42\times 1}$. This dataset contained roughly 250 metallic targets and 250 non-metallic targets. A detection scheme was chosen and performed on the entire dataset. The threshold needed to detect each object was determined and then a ROC curve was created based on how many metallic versus non-metallic targets were detected at each threshold.

To provide a more comprehensive view of performance for the MSD and CFAR detection schemes, they were applied after using three different types of downtrack filters. This was done to aid in isolating the detection results from the downtrack filter design, as well as to gain some insight into how well the new DCT AMF downtrack filter performed for detection. Detection results were also given for two other detection methods that are used in EMI processing in order to give a point of reference for the performance results of the proposed methods compared to current methods. All of these ROC curves are shown in Figure 6, where the title contains the downtrack filter method and the legend describes which detection method was used as well as the area under the given ROC curve. ROC curves with better performance will have an area closer to one, as one corresponds to perfect detection.

Each filter operates on the measurements contained in the previous 30 cm the sensor traversed. The first downtrack filter is a mean removal filter. The mean removal filter calculates the mean of the previous measurements at each frequency and then subtracts the mean from the current measurement. This filter serves as an example of using a downtrack filter design strictly to remove the self response. The second downtrack filter used in the comparison is the 30 cm wavelength sine filter. This sine filter is expected to be the closest option to a predetermined matched filter. The final downtrack filter is the DCT AMF that has been proposed in this work.

Six detection operations were applied after each of the aforementioned downtrack filters. The two baseline detection methods are the mean of the imaginary part of the frequency measurements and the ground removal method. The mean of the imaginary components of the frequency data is a baseline approach for detection that is used as the reference point in the results. The ground removal method depicted is performed by projecting the frequency data away from the soil response and then taking the power that is left in the measurements. This ground removal method can be used to quantify the level of improvement of the target detection by removing the soil interference term. Finally, the MSD and CFAR are applied to test their performance. Both the MSD and CFAR are run with the signal subspace containing five dimensions and nine dimensions. As mentioned before, this corresponds to a relative difference between the largest signal component and the noise floor of two and three significant digits. As a note of merit, the ground removal method is also equivalent to using the MSD approach and choosing the entire U projection as the signal subspace, or in other words, using all forty dimensions.

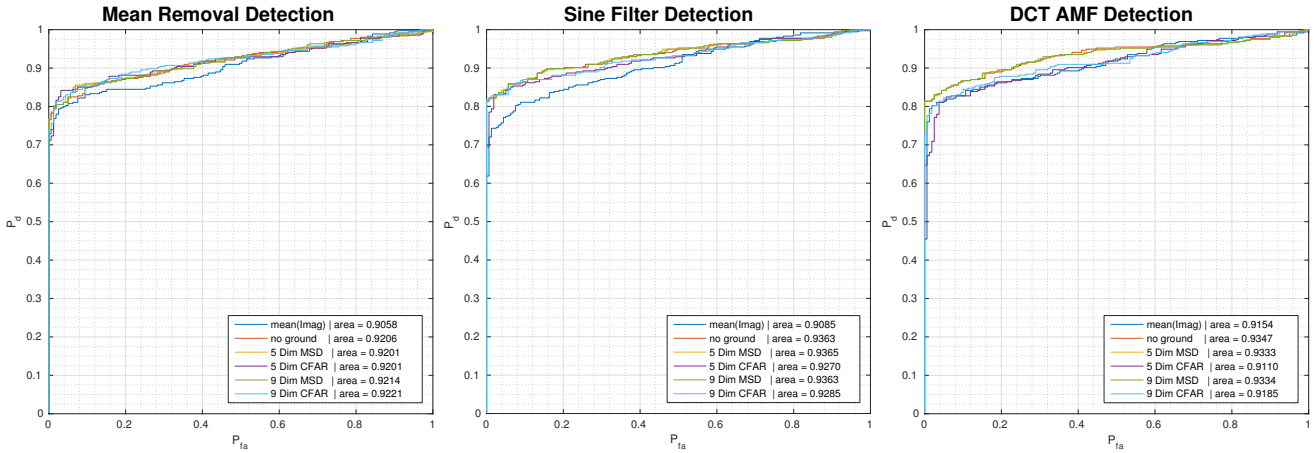

Figure 6. ROC curves with all possible combinations of six detection methods and three downtrack filters. Each graph contains the detection performance based on the chosen filter. The legends contain the area under the ROC curve for each filter-detection paring and can be used as a point of comparison, where 1 signifies perfect detection.

4.4 Observations

In order to interpret the results in Figure 6, it is useful to recall the optimality conditions of MSD and CFAR as well as some other contributing factors in these results. The MSD is optimal when the noise scaling factor is not changing. By relaxing this assumption for the CFAR method, it is also expected that the CFAR method will take a performance drop when this assumption holds true, but the more variance seen in the scaling factor will cause CFAR to out perform MSD. The difference in changing the dimensions of the MSD and CFAR will depend on how important the significant digits of the signal are in comparison with the noise floor. Also, when the noise floor is reduced to a sufficient degree, it is expected that ignoring the noise terms in the MSD will no longer have an effect as they are not interfering with the detection regardless.

The mean removal filter is a prime example of the expected results when the model includes a noise covariance with a varying scaling factor. In this case, all methods perform better than the baseline detection method. The nine dimensional MSD and CFAR perform the best. As can be seen in Figure 6, the CFAR outperforms the MSD, which implies that the varying scaling factor in the covariance is a more accurate model for the mean removal filter data. Finally, there is a performance drop from the nine dimensional MSD to the ground removal method. This implies that the noise level after the filter remains large enough to disrupt the detection metrics when the entire subspace orthogonal to the soil response is used.

The sine filter appears to illustrate the case where the model of a constant or only slightly varying noise covariance is occurring. The baseline detection using the imaginary data performs to the same degree as the mean removal filter and is the worst performing detection method for this filter. The MSD scheme is the best detection method for this downtrack filter. This implies that the covariance scaling term does not oscillate enough on this data set to require the added diversity of the model. Although this appears true for this dataset, it should be noted that this dataset was taken under the same operating conditions, at the same time, and with similar soil. A CFAR scheme may still be the optimal choice for a pre-trained threshold before the EMI platform is used in a new environment. Another interesting point is that the MSD performs nearly equivalent for all dimension options. This implies that the noise floor is reduced by the sine filter enough to not effect the detection metric to a significant degree.

The DCT AMF downtrack presents the most interesting results. The first artifact of note is that the DCT AMF is able to improve the target response in a manner that increases the performance of the baseline detection method compared to the alternative downtrack filters. Like the sine filter, the MSD response is consistent between dimensions. However the ground removal detection outperforms the nine dimensional MSD, which implies that useful information is contained in these lower dimensions that were of no value for previous downtrack filters. As for the decrease in performance of the MSD from the sine filter and most notably the decrease in the CFAR performance, it is the author's belief that these are due to the fact that the optimization problems will optimize some degree of the noise when there is no signal present. This would account for the slight decrease in performance with the ground removal detection between the sine filter and the DCT AMF. The CFAR suffers even more from this artifact because the noise that is optimized is strictly contained in the expected signal subspace. This causes the noise in the noise subspace to be smaller than that in the signal subspace when there is no target. Because CFAR uses the noise subspace to normalize the covariance scaling factor, this artifact serves to bias the detection such that noise can look like a weak target.

5. FUTURE WORK

The realization of the bias in the CFAR detection results for the DCT AMF downtrack filter approach has spurred the investigation of a way to mitigate this undesirable artifact. The artifact originates from the fact that the EMI processing uses the signal subspace projection $U_{\bar{G}S}$ in the frequency domain twice, once for the downtrack filter and then followed by the MSD or CFAR detection method. This creates two separate stages where the signal and noise subspace divide must be decided, and the added parameter choice only leads to more tuning parameters. In experiments that have been excluded from this work, the DCT AMF downtrack filter followed by the MSD or CFAR has shown to be fairly robust to the added tuning parameters, but it lends to the concern that the approach is suboptimal. It is of interest to find if the classical approach of using a two step process can in fact be reduced to a one step process. Initial experiments have confirmed this idea and a process

is being developed that simplifies the downtrack filtering and detection problem into a one step process. This can be accomplished by using the signal matrix $\mathbf{M}_S$ developed for the AMF filter and converting the matrix directly to a detection metric.

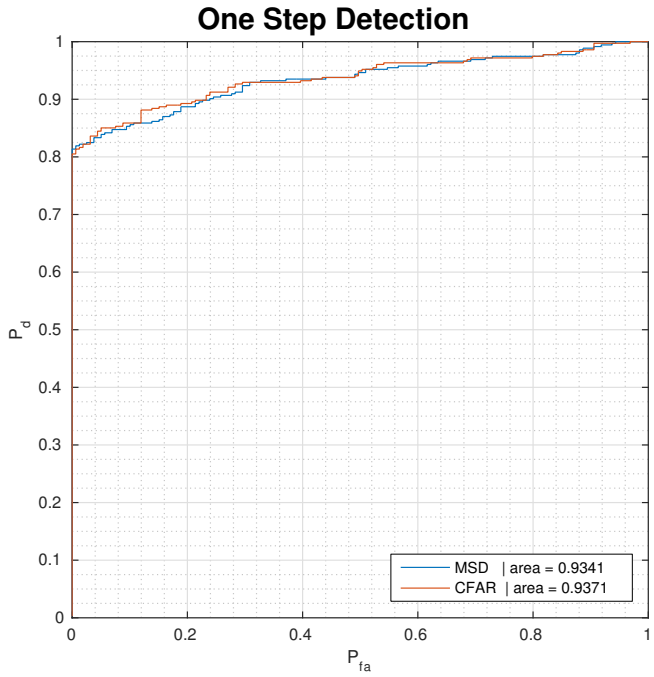

Figure 7. ROC curves showing the initial results from a one step process that converts the measurement matrix directly to a detection value.

A ROC curve from initial experiments is shown in Figure 7. This detection was run on the same dataset using a 30 cm long shifting window and used wavelengths of 5 cm and larger so as to be comparable to the previous results in Figure 6. As the one step formulation does not have an exact equivalent to any of the detection methods provided in the Figure 6, a simple MSD and CFAR detection was used. This future approach is revealing promising results as can be seen in Figure 7. The CFAR detection accuracy out performed any of the systems used in the previous results and the MSD was only out performed by the sine filter MSD. Future work will continue to validate this one step process as well as expand it to more EMI applications than the detection problem.

6. CONCLUSION

The first contribution this work has introduced is a method called the adaptive matched filter (AMF) that adaptively creates a downtrack filter for the EMI data. AMF is able to remove the sensor's self response interference while also improving the overall SNR of the frequency measurements. The new downtrack filter is designed in a way that it inherently avoids optimizing the interference soil response by isolating the desired target signal from the soil before creating the downtrack filter. The proposed AMF also has the flexibility to avoid enhancing noise by constraining the speed of oscillations allowed by the adaptive downtrack filter. These advances allow the AMF to be more robust to soil interference and noise than previous adaptive filter options. Furthermore, it was also shown to work equivalent to a current adaptive filter option when used on a dataset with minimal soil response interference in Figure 4.

The second contribution of this work has been to connect well developed detection theory directly to the EMI detection problem by using recent advances from Ref. 1 that make it possible to separate the frequency measurements into a signal, noise, and soil interference subspace. This work showed how the signal and noise subspace could be used to directly apply the Matched Subspace Detection methods of Ref. 2 to the EMI problem.

Results from a single dataset collected by the Georgia Tech wide-band EMI platform have been presented in Figure 6 to demonstrate the effectiveness of the proposed detection methods.

The final contribution of this work has been to show that it is possible to obtain improved results by moving away from the classical two step approach of wide-band EMI processing. The classical EMI strategy relies on a downtrack filter followed by processing in the frequency domain to perform the desired task. The new alternative uses a one step method to convert the measurement matrix $\mathbf{M}$ directly into the information for the desired task. Initial results from using a one step process for the detection problem were given in Figure 7. The detection capabilities of the one step process out performed any other method used on the dataset and show potential for the novel approach. Future work will continue to validate this new approach as well as extend it to more EMI processing applications.

Acknowledgment

This work is supported in part by the U.S. Army REDCOM CERDEC Night Vision and Electronic Sensors Directorate, Science and Technology Division, Countermine Branch and in part by the U. S. Army Research Office under Contract Number W911NF-11-1-0153.

REFERENCES

[1] C. E. Hayes, J. H. McClellan, and W. R. Scott, "Sparse recovery using an SVD approach to interference removal and parameter estimation," in *2015 IEEE Signal Processing & SP Education Workshop*, 2015.

[2] L. L. Scharf and B. Friedlander, "Matched subspace detectors," *Signal Processing, IEEE Transactions on*, vol. 42, no. 8, pp. 2146–2157, 1994.

[3] W. R. Scott, G. D. Larson, C. E. Hayes, and J. H. McClellan, "Experimental detection and discrimination of buried targets using an improved broadband CW electromagnetic induction sensor," pp. 90 720C–90 720C–15, 2014. [Online]. Available: http://dx.doi.org/10.1117/12.2050457

[4] G. Overton and C. Moreland, *Inside the Metal Detector*. Geotech, 2012.

[5] C. Bruschini, "A Multidisciplinary Analysis of Frequency Domain Metal Detectors for Humanitarian Demining," Ph.D. dissertation, Vrije Universiteit Brussel, 2002.

[6] M.-H. Wei, W. Scott, and J. McClellan, "Adaptive prefiltering for nonnegative discrete spectrum of relaxations," *Geoscience and Remote Sensing Letters, IEEE*, vol. 12, no. 5, pp. 1018–1022, May 2015.

[7] M. H. Wei, W. R. Scott, and J. McClellan, "Robust estimation of the discrete spectrum of relaxations for electromagnetic induction responses," *Geoscience and Remote Sensing, IEEE Transactions on*, vol. 48, no. 3, pp. 1169–1179, March 2010.

[8] S. Kraut, L. Scharf, and R. Butler, "The adaptive coherence estimator: a uniformly most-powerful-invariant adaptive detection statistic," *Signal Processing, IEEE Transactions on*, vol. 53, no. 2, pp. 427–438, Feb 2005.